Component Rearrangement on Printed Wiring Boards to Maximize the Fundamental Natural Frequency

Tien-Sheng Chang
Engineer,
Metal Industries Development Centre,
Taiwan, Republic of China

E. B. Magrab
Professor,
Department of Mechanical Engineering,
College of Engineering,
University of Maryland
College Park, MD 20742
Fellow ASME

A methodology to attain the highest fundamental natural frequency of a printed wiring board by rearranging its components has been developed. A general two-dimensional rearrangement algorithm is developed by which the rearrangement of the component-lead-board (CLB) assemblies is performed automatically for any combination of equal size, unequal size, movable and immovable CLBs. This algorithm is also capable of incorporating two design restrictions: fixed (immovable) components and prohibited (non-swappable) areas. A highly computationally efficient objective function for the evaluation of the automatic rearrangement process is introduced, which is a linear function of the size of the individual CLBs that have been selected for each interchange. The simulated annealing method is adapted to solve the combinatorial rearrangement of the CLBs. Using 61 combinations of boundary conditions, equal and unequal sized CLBs, movable and immovable CLBs, various CLB groupings and sets of material properties, it is found that, when compared to the exact solution obtained by an exhaustive search method, the simulated annealing method obtained the highest fundamental natural frequency within 1 percent for 87 percent of the cases considered, within 0.5 percent for 72 percent of the cases and the true maximum in 43 percent of them. To further increase the fundamental natural frequency the introduction of a single interior point support is analyzed. Depending on the boundary conditions an additional increase in the maximum fundamental natural frequency of 44 to 198 percent can be obtained.

Introduction

Integrated circuit technology has advanced rapidly in the past twenty years. The means to produce electronic equipment with high reliability and minimum overall cost has captured the attention of numerous researchers. Most of these researchers have been concerned with finding the optimal placement [1–6], minimum chip area [3, 7–9], and minimum wiring [10–12]. A few researchers have addressed different aspects of design optimization, such as the consideration of thermal properties [13–15], total failure rate [16], and optimal support location of a printed wiring board (PWB) [17].

Another important aspect of building reliable PWBs is to reduce the probability of failure due to mechanically generated motions, which can cause high relative displacement levels of the components and, consequently, high stress levels. These cyclic stress levels often lead to fatigue-induced cracked components and solder joints. One way to reduce the high cyclic stress is to subject the PWB to dynamic loadings whose frequency content is below the PWB's lowest natural frequency, thereby avoiding the amplification of the input displacements. Since, in a practical situation, the vibration environment is not within the designer's control, one seeks ways in which the fundamental natural frequency of the PWB can be raised as high as possible.

It is the objective of this research to use structural optimization techniques to determine how to rearrange the components of PWBs to attain its highest fundamental natural frequency for a given set of boundary conditions. In order to do this the following are required: (1) an efficient and accurate way of modeling the components comprising the PWB; (2) a finite element program to calculate the natural frequencies and mode shapes of the PWB for all combinations of boundary conditions; (3) a computationally efficient objective function to provide a basis for selecting among alternative configurations of the PWB; (4) a sophisticated scheme that can automatically rearrange any combination of equal, unequal, movable, and fixed (immovable) components; and (5) an optimization method that can find the global maximum.

In certain circumstances, however, the highest fundamental natural frequency obtained from the optimization method may not meet the desired minimum value. To further increase the fundamental natural frequency a way of automatically determining the location of a single interior point support for the previously determined optimal configuration is suggested.

Contributed by the Electrical and Electronic Packaging Division for publication in the JOURNAL OF ELECTRONIC PACKAGING. Manuscript received by the EEPD July 27, 1992; revised manuscript received March 31, 1993. Associate Technical Editor: P. Engel.

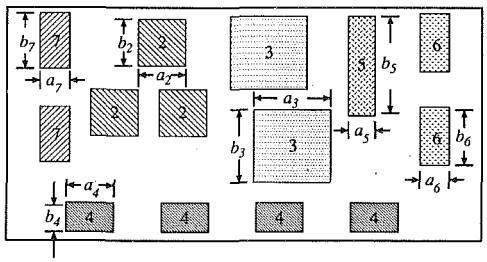

Fig. 1 An example of a PWB

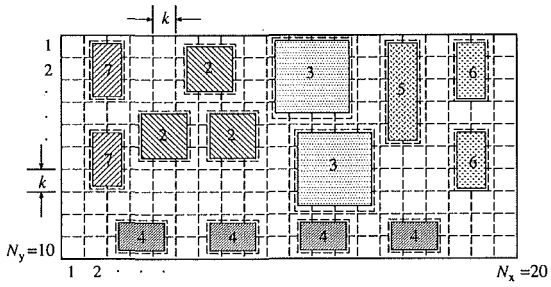

Fig. 2 Mesh generation prior to forming CLBs

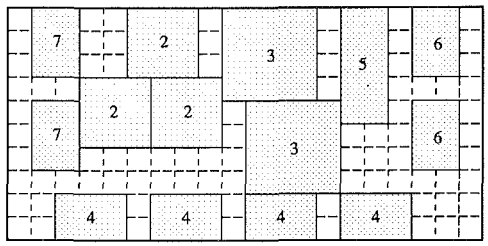

Fig. 3 Finite element model for PWB

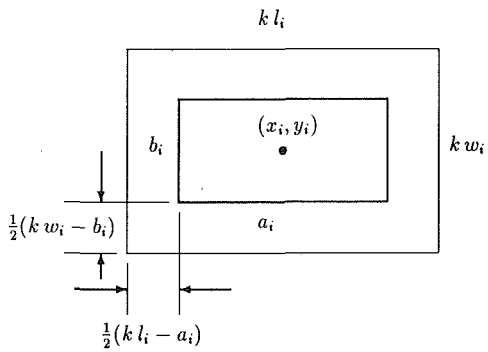

Fig. 4 Location of an individual component with respect to its CLB approximation

Modeling of the PWB

To reduce the complexity of the problem somewhat, the individual components and the PWB to which they are attached are first replaced by equivalent orthotropic plates [18–23], which are denoted component-lead-board (CLB) assemblies. The problem is now one of describing these CLBs in such a manner that they adequately represent the CLB's geometry, while still providing a reasonable means for their automatic rearrangement during the optimization process. In order to develop an algorithm for the rearrangement of the CLBs, these components are replaced with a simplified model that defines their type, the interaction between them, and their location. Such a model will reduce the complexity of the PWB, add structure to the problem, and make the optimal placement problem amenable to solution. After the algorithm is applied the results can be transformed back into their original description. The detailed transformation of the PWB structure into a finite element model is now described. The implications of these simplifications are discussed in the references cited above.

Consider a typical PWB shown in Fig. 1. The numbers 2 through 7 represent different types of components mounted on the board; that is, those with different material constants. Let the dimensions of the PWB be $a \times b$ and those of the individual components be $a_i \times b_i$. These dimensions are used to determine the size of the mesh for the subsequent finite element model such that all the a_i and b_i can be closely approximated by an integral number of elements. The PWB is now overlaid with a grid of square elements as shown in Fig. 2. The introduction of this square mesh is designed to reduce the complexity of the automatic rearrangement process, while still retaining a reasonable means of describing the geometry of the individual CLBs.

To avoid the possibility of any of the CLBs overlapping in the final configuration obtained from the automatic rearrangement process, the size of each individual CLB is enlarged to conform to its nearest exterior grid line as shown in Fig. 3. For those CLBs that have their dimensions equal to an integer multiple of the size of grid k, their position is relocated to the nearest grid line. Otherwise, their position is relocated to the center of the enlarged area as shown in Fig. 4. Hence, the PWB structure is simplified to an assemblage of square orthotropic and isotropic plate elements. The size of each CLB can now be expressed as the product of an integer multiple of square elements in the x-direction with an integer multiple of square elements in the y-direction as implied in Fig. 3 and shown in the second column of the Table 1.

Table 1 The equivalent sizes of the CLBs

CLB type (B_i)	No. of elements comprising each CLB type ($l_i \times w_i$)	Total number of CLBs N_i
1	1×1	83
2	3×3	3
3	4×4	2
4	3×2	4
5	2×5	1
6	2×3	2
7	2×3	2

The information in the second column of Table 1 is represented by two permanent arrays $\{P\}$ and $\{S\}$, whose lengths are equal to the total number N_d of CLB types, including the isotropic board. The total number of CLBs is

$$N_c = \sum_{i=1}^{N_d} N_i \tag{1}$$

For the example being considered $N_c = 97$ and $N_d = 7$. The elements in the $\{P\}$ array are the lengths l_i of the corresponding CLB type i. Similarly, the elements in the $\{S\}$ array are the widths w_i of the corresponding CLB type i. Thus, for the example given in Table 1,

$$\{P\} = \{l_1, l_2, \ldots, l_{Nd}\} = \{1,3,4,3,2,2,2\} \tag{2}$$

$$\{S\} = \{w_1, w_2, \ldots, w_{Nd}\} = \{1,3,4,2,5,3,3\} \tag{3}$$

The total number of each CLB type N_i is represented by a permanent array $\{R\}$ whose length is also equal to the total number N_d of CLB types. The elements in $\{R\}$ are

$$\{R\} = \{N_1, N_2, \ldots, N_{Nd}\} = \{83,3,2,4,1,2,2\} \tag{4}$$

The elements in each of these arrays are selected by the value of $B_i = i$. For example, if $i = 4$, then $B_4 = 4$ and $l_4 = 3$, $w_4 = 2$ and $N_4 = 4$. A number representing the corresponding CLB type is assigned to each individual square element of the

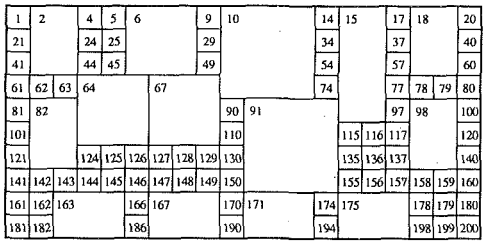

Fig. 5 Two dimensional representation of $\{L\}$

PWB. It is assumed that for those elements without any components mounted to them they are the board itself, and are denoted as CLB type 1. Consequently, the configuration of the original PWB shown in Fig. 1 has been modeled as $N_x \times N_y$ square elements, where the total number of grids is

$$N_{xy} = N_x N_y = \sum_{i=1}^{N_d} w_i l_i N_i \tag{5}$$

A two-dimensional array, denoted the content matrix $\tilde{C}$, is constructed to store the corresponding type number of each individual element of the current configuration. Thus $C_{ij} = B_n$ where $n = 1, 2, \ldots, N_d$. For the original PWB shown in Fig. 1, $\tilde{C}$ is given by:

$$\begin{bmatrix}
1 & 7 & 7 & 1 & 1 & 2 & 2 & 2 & 1 & 3 & 3 & 3 & 3 & 1 & 5 & 5 & 1 & 6 & 6 & 1 \\
1 & 7 & 7 & 1 & 1 & 2 & 2 & 2 & 1 & 3 & 3 & 3 & 3 & 1 & 5 & 5 & 1 & 6 & 6 & 1 \\
1 & 7 & 7 & 1 & 1 & 2 & 2 & 2 & 1 & 3 & 3 & 3 & 3 & 1 & 5 & 5 & 1 & 6 & 6 & 1 \\
1 & 1 & 1 & 2 & 2 & 2 & 2 & 2 & 2 & 3 & 3 & 3 & 3 & 1 & 5 & 5 & 1 & 1 & 1 & 1 \\
1 & 7 & 7 & 2 & 2 & 2 & 2 & 2 & 2 & 1 & 3 & 3 & 3 & 3 & 5 & 5 & 1 & 6 & 6 & 1 \\
1 & 7 & 7 & 2 & 2 & 2 & 2 & 2 & 2 & 1 & 3 & 3 & 3 & 3 & 1 & 1 & 1 & 6 & 6 & 1 \\
1 & 7 & 7 & 1 & 1 & 1 & 1 & 1 & 1 & 1 & 3 & 3 & 3 & 3 & 1 & 1 & 1 & 6 & 6 & 1 \\
1 & 1 & 1 & 1 & 1 & 1 & 1 & 1 & 1 & 1 & 3 & 3 & 3 & 3 & 1 & 1 & 1 & 1 & 1 & 1 \\
1 & 1 & 4 & 4 & 4 & 1 & 4 & 4 & 4 & 1 & 4 & 4 & 4 & 1 & 4 & 4 & 4 & 1 & 1 & 1 \\
1 & 1 & 4 & 4 & 4 & 1 & 4 & 4 & 4 & 1 & 4 & 4 & 4 & 1 & 4 & 4 & 4 & 1 & 1 & 1
\end{bmatrix} \tag{6}$$

We now form a one-dimensional location array $\{L\}$, whose length is equal to the total number of CLBs N_c. The purpose of $\{L\}$ is to record only the upper-left corner address number in the content matrix $\tilde{C}$ corresponding to each individual CLB type for the current configuration. For the example shown in Fig. 5

$$\{L\} = \{1,2,4,5,6,9,10,14,15,17,18,20,21,24,25, \ldots, 194,198,199,200\} \tag{7}$$

Thus, the grid number of the upper left-hand corner of the individual CLBs for the current arrangement is registered as a single integer number from 1 to N_{xy}. During the automatic rearrangement process only the integer numbers stored in array $\{L\}$ can be accessed. For each selected number one obtains the CLB type from the content matrix $\tilde{C}$ and the corresponding dimensions l_i and w_i from the arrays $\{P\}$ and $\{S\}$, respectively. In this manner the connectivity of each CLB is maintained during the rearrangement process. For each L_k selected the coordinates of the corresponding element in $\tilde{C}$ are obtained as follows:

$$i = 1 + \text{INTEGER}\left[\frac{L_k - 1}{N_x}\right] \tag{8}$$

$$j = L_k - (i-1)N_x \tag{9}$$

The PWB structure has now been transformed into a finite element model consisting of square orthotropic and isotropic elements, and its configuration can be fully described by the associated content matrix $\tilde{C}$, the location index array $\{L\}$ and the equivalent CLB dimensions in arrays $\{P\}$ and $\{S\}$.

Immovable CLBs and Restricted Areas

In the design of a PWB some of the CLBs, say M of them, may not be allowed to be relocated in the rearrangement process. In this case the corresponding grid numbers are removed from the array $\{L\}$ and the length of the location array $\{L\}$ becomes $N_c = N_c - M$. It is also possible that certain areas of the PWB may be prohibited from having any components placed there. Again, the grid numbers for these prohibited areas are removed from the array $\{L\}$ and N_c is again reduced. The size of the rearrangement process problem shrinks when these types of design constraints are prescribed.

Geometric Constraints

CLBs Must be Distinct. When two numbers are chosen from the location array $\{L\}$ the two grid numbers are transformed to two elements of matrix $\tilde{C}$ to obtain the corresponding CLB type using Eqs. (8) and (9). The interchange of these two CLBs is performed only when they are distinct; that is, their type number is different. For example, if the two integer numbers selected, which must be between 1 and N_c, are 5 and 31, then the corresponding grid numbers are found from array $\{L\}$ to be 6 and 67, respectively. Since the CLB type for both grid numbers is type 2 no interchange would be performed.

Boundary Constraints. When two CLBs are found to be distinct and their sizes are feasible, the boundary constraints are then checked. Again, let the number of finite elements along the x- and y-directions of these two CLBs be l_1 and w_1 and l_2 and w_2, respectively. Assume that the numbers selected are located on the i_1th and the i_2th rows and j_1th and j_2th columns in the content matrix $\tilde{C}$, respectively. Consider the case wherein the selected CLBs satisfy Eq. (10). An intended rectangular or square swapping area for the first CLB type is defined by the subscripts of the elements in the content matrix $\tilde{C}$, which range from (i_2, j_2) to $(i_2 + w_1 - 1, j_2 + l_1 - 1)$. The first pair of subscripts defines the rectangle's (or square's) upper left-hand corner and the second pair its lower right-hand corner. Referring to Fig. 6 it is seen that there are two intended swapping areas for each pair of CLBs. Only the intended swapping area for the larger CLB is checked to determine if it satisfies the boundary constraints. Notice that the actual size for both swapping areas is determined by the size of the larger CLB; that is, $w_1 \times l_1$ for the example shown in Fig. 6. The detailed procedures and example for checking the boundary constraints are given in what follows.

The boundary constraints can be expressed along the x-axis as:

$$j_2 + l_1 - 1 \le N_x \tag{10}$$

and along the y-axis as

$$i_2 + w_1 - 1 \le N_y \tag{11}$$

An example of an infeasible interchange due to the boundary constraints is given as follows. Consider Fig. 7(*a*) and assume that two numbers 7 and 64 are chosen, and that they correspond to the numbers 10 and 143, respectively, in the location index array $\{L\}$. The corresponding locations in the content matrix

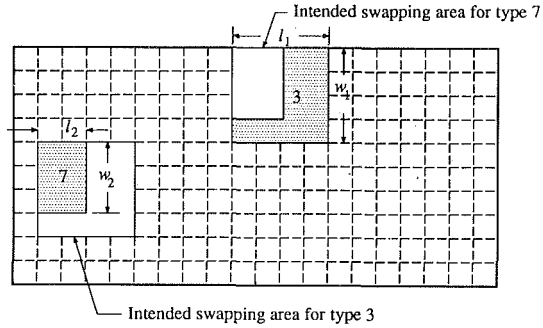

Fig. 6 Definition of the intended swapping areas

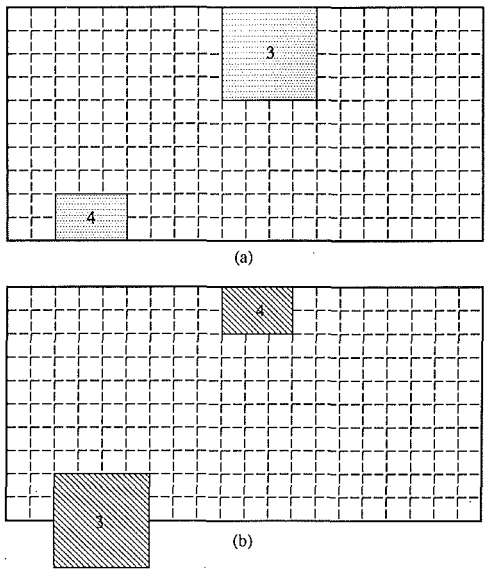

Fig. 7 Contradiction due to the boundary constraints. (*a*) Original configuration, (*b*) intended swapped configuration

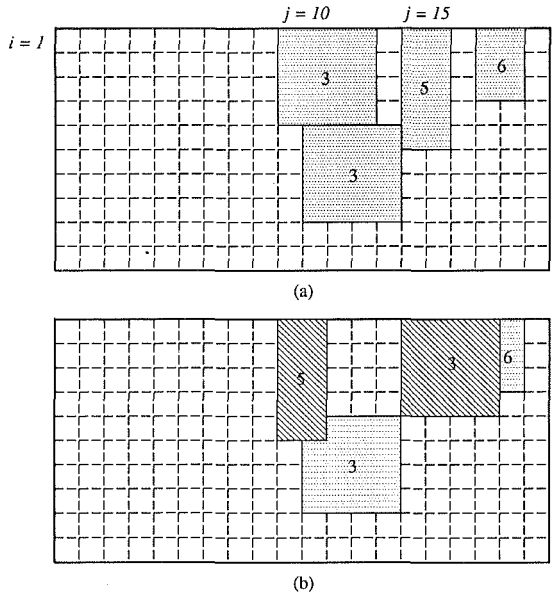

Fig. 8 Contradiction to the feasibility of the size of a CLB. (*a*) Original configuration, (*b*) infeasibility of intended swap

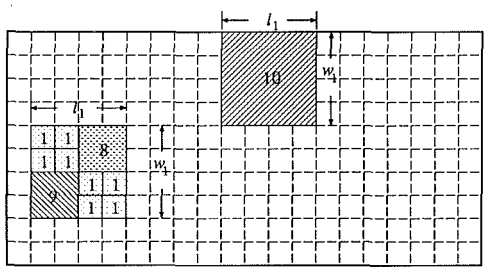

Fig. 9 Example of a feasible interchange between two areas

$\tilde{C}$ are found to be (1, 10) and (8, 3), respectively, and the CLB types are 3 and 1, respectively. From arrays $\{P\}$ and $\{S\}$ the sizes of these two types of CLBs are 4 × 4 and 1 × 1, respectively. From Eq. (10) the feasibility of the sizes of these two CLBs is satisfied. The intended square swapping area for the CLB of type 3 has its upper left-hand corner at (8, 3) and its lower right-hand corner at (11, 6) in the content matrix $\tilde{C}$. It is clear that this interchange process contradicts Eq. (12). The interchange of these two CLBs would have placed one of the CLBs outside the boundary as shown in Fig. 7(*b*).

Feasibility of the Size. Consider two different type CLBs for which the number of the finite elements along the *x*- and *y*-directions are l_1 and w_1 and l_2 and w_2, respectively. The interchange of these two CLBs is feasible only when either

$$l_1 \geq l_2 \quad \text{and} \quad w_1 \geq w_2 \tag{12}$$

or

$$l_1 \leq l_2 \quad \text{and} \quad w_1 \leq w_2 \tag{13}$$

are true.

An example of an infeasible interchange due to the CLB sizes is given as follows. Consider Fig. 8(*a*) and suppose that the numbers 7 and 9 have been selected and they correspond to the index numbers 10 and 15 in the one-dimensional array $\{L\}$. The locations in $\tilde{C}$ are (1, 10) an (1, 15), respectively. The corresponding types of the CLBs are found to be type 3 and 5, respectively. From arrays $\{P\}$ and $\{S\}$ it is found that the sizes of these two types of CLBs are 4 × 4 and 2 × 5, respectively; that is, $l_1 = 4$, $w_1 = 4$, $l_2 = 2$, and $w_2 = 5$. It is found that neither Eq. (10) nor Eq. (11) is satisfied and, therefore, the interchange is not allowed. The interchange of these two CLBs would have resulted in their overlapping other CLBs as shown in Fig. 8(*b*).

CLB Must be Containable. It is possible that the intended swapping areas could contain other CLBs, in addition to the one that is chosen. The intended swapping areas, therefore, are checked to see whether or not they are containable. In other words, to determine if an integral number of CLBs and board elements of size 1 × 1 fit inside their respective intended swapping areas. This concept of containability is especially important when performing the rearrangement of CLBs of unequal size. For example, if the intended swapping area is l_1 × w_1 as shown in Fig. 9, then their interchange is feasible only when $(i - 1) \times N_x + j = L_k$, $k = 1, \ldots, N_c$ and both of the following equations are satisfied:

$$j + l_\alpha \leq l_1 + j_2 \tag{14}$$

and

$$j + w_\alpha \leq w_1 + i_2 \tag{15}$$

where $\alpha = B_\alpha = C_{ij}$, for $i = i_2, \ldots, i_2 + w_1 - 1$ and $j = j_2, \ldots, j_2 + l_1 - 1$. In other words, only the upper left-hand corner element of each individual CLB inside the intended swapping area is checked. For the example shown in Fig. 9, the containability criterion is satisfied since an integral number of CLBs fit inside the intended swapping areas.

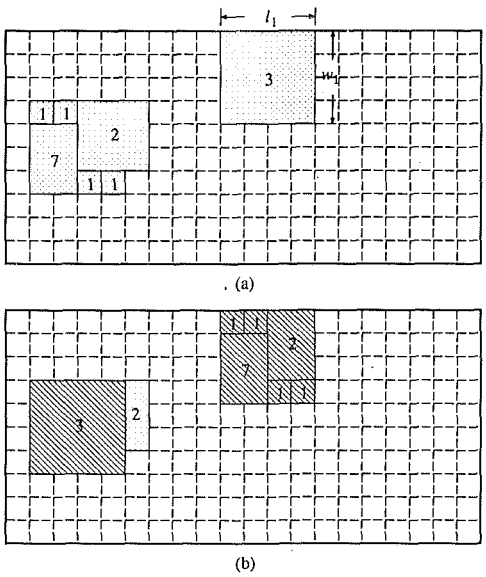

Fig. 10 Contradiction to the containable property. (*a*) Original configuration, (*b*) intended swapped configuration

An example of an infeasible interchange of two CLBs due to the contradiction of the containable property is given as follows. Assume that two numbers 7 and 28 are selected. Their corresponding index numbers in the location index array $\{L\}$ are 10 and 62, respectively. The locations in the content matrix $\tilde{C}$ are (1, 10) and (4, 2), respectively, and the corresponding CLB types are 3 and 1, respectively, as shown in Fig. 10(*a*). From arrays $\{P\}$ and $\{S\}$ the size of these two types of CLBs are 4 × 4 and 1 × 1, respectively. It is seen from Eq. (10) that the feasibility of the sizes of these two CLBs is satisfied. The intended swapping square area for the CLB of type 3 has its upper left-hand corner at (4, 2) and its lower right-hand corner at (7, 5) in the content matrix $\tilde{C}$. The boundary constraints given by Eqs. (12) and (13) are also satisfied. Equations (14) and (15) are therefore checked for their containability. It is found that the intended interchange contradicts Eq. (15) when i and j equal to 1 and 3, respectively. The interchange of these two CLBs would have overlapped and split other CLBs as shown in Fig. 10(*b*).

Transformation of Finite Element Model to Component's Location. As shown in Fig. 4 the location of each individual CLB is at the center of its area $(kl_i) \times (kw_i)$. The final configuration obtained from the automatic rearrangement and optimization process must be transformed back to their actual sizes on the PWB. To do this the grid numbers for the finite element model and their associated connectivity are converted to their x_i, y_i coordinates using the original dimensions a_i and b_i of each CLB. For example, consider a CLB that has its upper left-hand corner index located at (i, j) in the content matrix $\tilde{C}$. Let the number of elements along the x- and y-directions for this CLB type be l and w, respectively. The actual dimensions of this CLB were stored as a' and b'. The actual coordinates of the location of the upper left-hand corner (U_x, U_y) of this CLB are therefore

$$U_x = (j-1)k + \frac{1}{2}(kl - a') \tag{16}$$

$$U_y = (i-1)k + \frac{1}{2}(kw - b') \tag{17}$$

and the coordinates of its center are

$$x_i = (j-1)k + \frac{kl}{2} \tag{18}$$

$$y_i = (i-1)k + \frac{kw}{2} \tag{19}$$

Objective Function

The fundamental natural frequency can be approximated by the Rayleigh quotient

$$\omega_1^2 = \frac{\int_0^a \int_0^b U dxdy}{\int_0^a \int_0^b \hat{T} dxdy} \tag{20}$$

where, for an orthotropic plate the quantities U and $\hat{T}$ are given by

$$U = D_x\left(\frac{\partial^2 W_1}{\partial x^2}\right)^2 + 2D_c\left(\frac{\partial^2 W_1}{\partial x^2}\right)\left(\frac{\partial^2 W_1}{\partial y^2}\right) + D_y\left(\frac{\partial^2 W_1}{\partial y^2}\right)^2 + 4D_{xy}\left(\frac{\partial^2 W_1}{\partial x \partial y}\right)^2 \tag{21}$$

$$\hat{T} = \rho h W_1^2 \tag{22}$$

and $W_1 = W_1(x, y)$ is the plate's mode shape corresponding to its fundamental natural frequency ω_1, ρ and h are the mass density per unit volume and thickness of the plate, respectively, and D_x, D_y, D_{xy}, and D_c are the flexural rigidities of the orthotropic plate [22]. The right-hand side of the Eq. (20) is known as the Rayleigh Quotient for an orthotropic plate. It is well known that a good estimation of the fundamental natural frequency is obtained when the approximate displacement function $W_1(x, y)$ satisfies the boundary conditions and closely resembles the actual fundamental mode shape.

It can be shown [24] that the numerator and denominator of Eq. (20) can be approximated by

$$\omega_1^2 = \frac{U_0}{\hat{T}_0} = \sum_{i=1}^{N_y}\sum_{j=1}^{N_x} U_{ij}(C_{ij}) \Big/ \sum_{i=1}^{N_y}\sum_{j=1}^{N_x} \hat{T}_{ij}(C_{ij}) \tag{23}$$

where

$$U_{ij}(C_{ij}) = (D_x)_{C_{ij}}(S_1)_{ij} + (D_c)_{C_{ij}}(S_2)_{ij} + (D_y)_{C_{ij}}(S_3)_{ij} + (D_{xy})_{C_{ij}}(S_4)_{ij} \tag{24}$$

$$\hat{T}_{ij}(C_{ij}) = (\rho h)_{C_{ij}}(S_5)_{ij} \tag{25}$$

$$(S_1)_{ij} = \left(\frac{\partial^2 W_1}{\partial x^2}\right)_{ij}^2 \tag{26}$$

$$(S_2)_{ij} = 2\left(\frac{\partial^2 W_1}{\partial x^2}\right)_{ij}\left(\frac{\partial^2 W_1}{\partial y^2}\right)_{ij} \tag{27}$$

$$(S_3)_{ij} = \left(\frac{\partial^2 W_1}{\partial y^2}\right)_{ij} \tag{28}$$

$$(S_4)_{ij} = 4\left(\frac{\partial^2 W_1}{\partial x \partial y}\right)_{ij}^2 \tag{29}$$

$$(S_5)_{ij} = (W_1^2)_{ij} \tag{30}$$

and it was assumed that $dxdy \Rightarrow \Delta x\, \Delta y = k^2$. The subscripts i and j indicate the location of each $k \times k$ element in the $\tilde{C}$ matrix. The subscript C_{ij} denotes the material properties corresponding to that element.

To determine a good estimate of $W_1(x, y)$ the finite element approximation to the original configuration is used. For moderate changes in the properties of a structure it is reasonable to assume that $W_1(x, y)$ does not change. Furthermore, the second derivatives of the transverse displacement can be approximated by the appropriate linear combination of the modal displacements determined from the finite difference method [25]. These linear combinations are a function of the plate's boundary conditions for those elements that are on the plate's

perimeter. Since W_1 is assumed to remain constant throughout the design changes, these approximations to the second derivatives are only computed one time. Therefore, the $(S_k)_{ij}$, $k = 1, 2, \ldots, 5$, are constants. The evaluation of $U_{ij}(C_{ij})$ for each individual element for the finite element model contains only four multiplications and three additions. The evaluation of $\hat{T}_{ij}(C_{ij})$ requires one multiplication.

Consider the mathematical operations required for the evaluation of the design changes using this proposed objective function. Let two sets of $l_1 \times w_1$ elements be exchanged as shown in Fig. 9. One set has the original location of its elements defined by the indices $i = I_1, \ldots, I_1 + w_1 - 1$ and $j = J_1, \ldots, J_1 + l_1 - 1$, whereas that of the second set by $i = I_2, \ldots, I_2 + w_1 - 1$ and $j = J_2, \ldots, J_2 + l_1 - 1$. We now define several quantities as follows:

$$U_s^t = \sum_{i=I_s}^{I_s+w_1-1} \sum_{i=J_s}^{J_s+l_1-1} U_{ij}(C_{ij}^t) \tag{31}$$

$$\hat{T}_s^t = \sum_{i=I_s}^{I_s+w_1-1} \sum_{i=J_s}^{J_s+l_1-1} \hat{T}_{ij}(C_{ij}^t) \tag{32}$$

where C_{ij}^t, $t = 1, 2$ denotes the element of content matrix $\tilde{C}$ for the current and new configurations, respectively, and $s = 1, 2$ denotes the location indices for the two sets of elements to be exchanged. It is now possible to compute a new estimate of the fundamental natural frequency ${\omega_1'}^2$ from the following expression:

$${\omega_1'}^2 = \frac{U_0 + (U_1^2 - U_1^1) + (U_2^2 - U_2^1)}{\hat{T}_0 + (\hat{T}_1^2 - \hat{T}_1^1) + (\hat{T}_2^2 - \hat{T}_2^1)} \tag{33}$$

In Eq. (33) both U_0 and $\hat{T}_0$ are computed only one time. All subsequent computations involve only U_s^t and $\hat{T}_s^t$. Since detection of any improvement of a new configuration can be determined from Eq. (33) during the interchange process, the objective function F of the current configuration is set to the negative of ω_1^2; that is [recall Eq. (23)]

$$F = -\frac{U_0}{\hat{T}_0} \tag{34}$$

The comparison between a pair of configurations can be made by simply computing the difference in the objective function shown in Eq. (33) with that obtained with Eq. (34). Suppose, for example, that during the rearrangement process the two sets of elements to be interchanged are the two $l \times w$ areas shown in Fig. 6. The justification for accepting the interchange of these two areas only requires the computation of the quantities shown in Eqs. (31) and (32) with $l = 4$, $w = 4$, $J_1 = 10$, $I_1 = 1$, $J_2 = 2$, and $I_2 = 5$. The value of the objective function for the new configuration F' is then determined from

$$F' = -\frac{U_a}{\hat{T}_a} = -{\omega_1'}^2 \tag{35}$$

The fundamental natural frequency for the swapped configuration has increased when $F' < F$. In this case, the swapped configuration is retained and the values of the U_0 and $\hat{T}_0$ are set equal to U_a and $\hat{T}_a$, respectively. The current configuration is restored when $F' \geq F$ and the quantities U_0 and $\hat{T}_0$ remain the same.

Empirical Formulation for Simulated Annealing

Simulated annealing is a technique for solving the combinatorial optimization problems [26]. The objective function of an optimization problem is analogous to the energy in a physical system, and the interchanges between components to attain new configurations are analogous to the changes in the energy state of the physical system. Interchanges are selected randomly and the possibility of accepting a move is dependent of the system's current temperature[1], which is controlled by a probability function using the Metropolis algorithm [27]. The analogy between simulated annealing and the PWB optimal placement problem is given in Table 2.

Table 2 Analogy between simulated annealing and the PWB optimal placement problem

Simulated annealing	⇒	PWB optimal placement
Energy (E)	⇒	Objective function ($F = -\omega_1^2$)
Energy state	⇒	Configuration of PWB
Crystalline solid state	⇒	Optimal placement of PWB
Cooling schedule	⇒	Search procedure
Temperature	⇒	Scaling factor of ω_1^2, T
Initial temperature	⇒	Initial scaling factor of ω_1^2, T_i
Cooling temperature factor	⇒	Control parameter, T_c
Final temperature	⇒	Stopping criterion of scaling factor, T_f

The performance of the simulated annealing method, as measured by the quality of the solution and the overall computational time, is dependent on the search procedure, the initial value of the scaling factor T, denoted T_i, the control factor T_c and the stopping criterion of scaling factor T_f. After some computational experience was obtained it was found that

$$T_i = 0.01 |FN_{bd}| \tag{36}$$

where N_{bd} is the number of zero finite element nodal displacements of the prescribed boundary conditions and F is obtained for the initial configuration from Eq. (34).

The annealing process is completed when the value of the scaling factor T is such that virtually no configuration changes will occur. After some numerical testing for the PWB optimal placement problem the stopping criterion for the scaling factor T, denoted T_f, was set to $T_f = 10^{-20}$. However, since the value of the scaling factor varies with the boundary conditions and the total number of CLBs considered, the optimal configuration can be obtained before this pre-selected value T_f is reached, and, therefore, unnecessary searching time will have taken place. To avoid this situation a quantity that records the number of successful swaps N_{su} at each value of T is introduced to serve as an additional stopping criterion. The searching process is terminated when either T_f is reached or no successful swap occurs at the current value of the scaling factor T; that is, when either $T = T_f$ or $N_{su} = 0$.

The value of scaling factor T of the simulated annealing method is decreased gradually by a factor of T_c. Empirically, in order to allow the value of T to decrease slowly, it has been suggested that T_c vary between 0.8 to 1.0 for the combinatorial optimization problem [3]. In this research the factor is set to $T_c = 0.9$; that is $T_{new} = 0.9\ T_{old}$.

The maximum number of configuration swaps allowed for each value of T is, therefore, controlled by the maximum number of tries $(N_{try})_{max}$ and the maximum number of successful swaps $(N_{su})_{max}$. It has been found that the maximum number of tries and the maximum number of successful swaps for each value of T are a function of N_c. Therefore, both of these numbers were set to $(N_{su})_{max} = (N_{try})_{max} = 50\ N_c$. A typical curve of the number of successful swaps at each T versus the value of T is given in Fig. 11 for four different boundary conditions. As seen in the figure, the choice of the initial value of the scaling factor T_i is a function of the boundary conditions. The final value of the scaling factor T_f also varies with the boundary conditions. Notice that the determination of the initial value T_i given by Eq. (36) is an empirical formula. It suggests a value for the initial scaling factor T_i that is high enough, but not unnecessarily high, for this PWB optimal placement problem.

[1]When using simulated annealing it is conventional to refer to the value of the objective function as temperature. In the present problem temperature corresponds to ω_1^2.

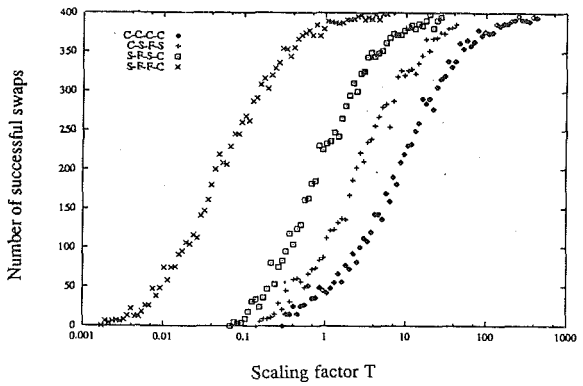

Fig. 11 Typical curve of temperature versus the number of successful swaps for simulated annealing for various boundary conditions and for $N_c = 8$ [$(N_{try})_{max} = (50)(N_c) = 400$]

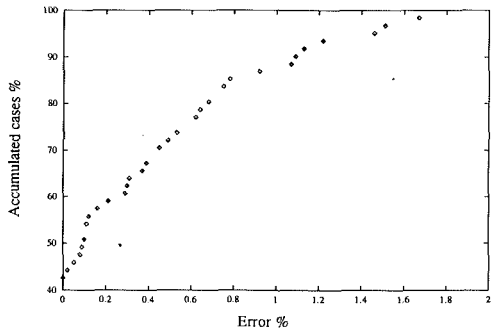

Fig. 12 The percentage error between the highest fundamental natural frequencies found by the simulated annealing and the exact maximum fundamental natural frequencies obtained from the exhaustive search method versus the percentage of total number of cases less than that error. A total of 61 different cases were considered.

Table 3 Characteristics of the CLBs for the five examples

Example	Size of CLBs	Mass density	Rigidities	Mobility
1	Equal	Equal	Various	All movable
2	Equal	Various	Equal	All movable
3	Equal	Various	Various	All movable
4	Unequal	Various	Various	One immovable
5	Unequal	Various	Various	Some movable

Table 4 The boundary conditions

Case	Edge 1	Edge 2	Edge 3	Edge 4
1	Clamped	Clamped	Clamped	Clamped
2	Simple	Clamped	Simple	Clamped
3	Clamped	Clamped	Clamped	Free
4	Clamped	Free	Clamped	Free
5	Clamped	Simple	Free	Simple
6	Simple	Free	Simple	Clamped
7	Simple	Free	Simple	Free
8	Simple	Free	Free	Clamped

Exhaustive Search Method

An exhaustive search method [25] was used to determine the exact global optimal configuration of the components on the PWB for several very small combinatorial problems. To obtain an exact solution for the global optimal configuration of the PWB, an algorithm [25] was developed that generated all the possible distinct configurations. A standard finite element method was used to determine the fundamental natural frequency of each individual configuration obtained from the permutation process. The optimal configuration corresponding to the highest fundamental natural frequency was then obtained by sorting all the fundamental natural frequencies from high to low. The number of distinct component combinations in these small combinatorial problems varied from 648 to 92,544.

Examples and Comparison

To demonstrate that the suggested cooling schedule and objective function can be used to search for the optimal configuration of the PWB for various combinations of the equal size, unequal size, movable and immovable CLBs and for various boundary conditions in a relatively short computational time, five examples are investigated. These examples include those in which the CLBs have either uniform mass density and varying rigidities, uniform rigidities and varying densities, or varying mass densities and rigidities. The general characteristics of the CLBs for the five cases to be rearranged are shown in Table 3, as are the cases that have movable and immovable CLBs. The various combinations of boundary conditions considered are shown in Table 4. Each example is conducted on an 8 × 6 in. PWB that is modeled[2] by 48 1 × 1 in. finite element squares ($k = 1$ in.) When the results obtained from the simulated annealing were compared with those using the exhaustive search method, the simulated annealing method found the highest fundamental natural frequency $\omega_1' = \omega_1/\sqrt{(\rho h)_1}$ within 1 percent for 87 percent of the cases considered, within 0.5 percent for 72 percent of them and the true maximum in 43 percent of the cases. The cumulative distribution of the number of cases as a function of the percentage error is shown in Fig. 12. These cases considered 61 combinations of the boundary conditions, equal and unequal sized CLBs, movable and immovable CLBs, various grouping types and several sets of material constants. When the 61 combinations were re-run using a different set of randomly determined rearrangements these percentages remained virtually the same. For those few results obtained by the simulated annealing that did not converge to the highest fundamental natural frequency it is possible that:

1. Since the possible configurations are generated randomly some configurations may not have been generated during the search process.
2. Since the number of tries (N_{try}) is a relatively small value that has been chosen to prevent the possibility of lengthy computational time, when the total possible number of permutations becomes large the probability of finding the global maximum decreases.

It was found that in 3 out of the 8 cases in which the simulated annealing found the highest fundamental natural frequency to be more than 1 percent lower than the global maximum, they still ranked within the 10 highest exact fundamental natural frequencies. In 8 out of the 9 cases in which the simulated annealing found the highest fundamental natural frequency within 0.5 to 1 percent of the global maximum, they also ranked within the 10 highest fundamental natural frequencies. The maximum error was slightly less than 3 percent. Therefore, the suggested cooling schedule, which uses the energy for the initial configuration, the number of zero finite element nodal displacements from the prescribed boundary conditions and total number of the individual CLBs, seems to be both efficient and accurate enough for searching for the optimal configuration for all the combinations of the PWB placement problems considered. It also seen that the modified Rayleigh procedure given by Eqs. (23) to (34) is a very accurate predictor of ω_1^2.

An Application

The optimization method presented is now applied to an

[2]When the fundamental natural frequency for several of these cases was evaluated it was found that an increase in the number of elements from 48 to 96 resulted in the value of the natural frequency changing by approximately 0.1 percent. Thus, 48 elements were considered adequate.

Table 5 Material constants [17] for the CLB type in Table 1 and Figure 3

Component	CLB type	D_x	D_y	D_{xy}	D_c	$\rho h(\times 10^{-5})$
Board	1	56.75	56.75	19.86	17.03	3.109
Capacitor	2	56.75	56.75	19.86	17.03	14.767
Capacitor	3	56.75	56.75	19.86	17.03	19.948
Transformer	4	52.56	167.93	34.03	15.77	31.865
Heat sink	5	102.73	53.38	27.84	16.07	30.311
Transformer	6	66.75	112.10	32.35	20.03	9.585
Chip socket	7	215.40	79.72	48.40	23.92	3.109

Table 6 Highest fundamental natural frequency and corresponding CPU time

Boundary conditions	Initial frequency (Hz)	Maximum frequency (Hz)	Percentage improvement	CPU time* (seconds)
C-C-C-C	108.08	204.45	89.17	137.7
S-C-S-C	106.54	150.26	41.04	476.2
C-C-C-F	33.86	64.97	91.88	61.5
C-F-C-F	21.47	36.95	72.10	84.4
C-S-F-S	48.05	71.84	49.51	79.2
S-F-S-C	21.11	49.07	132.45	64.9
S-F-S-F	9.22	14.43	56.51	91.9
S-F-F-C	16.64	38.63	132.15	77.0

*SUN 4/75 (SPARC 2).

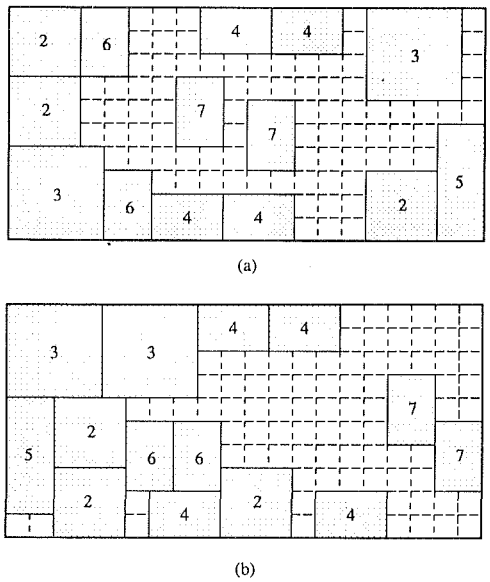

Fig. 13(*a*) Optimized configuration for C-C-C-C boundaries, (*b*) optimized configuration for C-S-F-S boundaries

example in which experimentally determined material constants [17] are used, and in which several combinations of the boundary conditions are considered. This example considers the rearrangement of seven unequal size CLBs. The PWB shown in Fig. 3, which is approximated as a finite element model shown in Fig. 4, is used as the initial configuration for all the combinations of the boundary conditions considered. The flexural rigidities (lbf-in.) and mass density per unit area (lb–s^2/in.^{3}) for each individual CLB type are given in Table 5. The corresponding size and number of each CLB type are given in Table 1. The size of the PWB is 10 × 5 in. All the CLBs can be relocated and no prohibited areas are prescribed. The highest fundamental natural frequencies corresponding to eight sets of the boundary conditions and the fundamental natural frequency for the initial configuration are given in Table 6. Two configurations corresponding to the optimal natural frequency for boundary conditions "C-C-C-C" and "C-S-F-S" are shown in Figs. 13 (*a*) and (*b*), respectively. From Table 6 it is seen that the fundamental natural frequencies for the boundary conditions considered were increased by 41 to 132 percent from their initial configurations.

A Method to Further Increase the Fundamental Natural Frequency

In certain circumstances the highest fundamental natural frequency obtained from the optimization method described may not meet the desired minimum value, and further improvement is needed. One strategy that can be used to increase the fundamental natural frequency further is to introduce a point support somewhere on the plate. To determine the location and the effect that the placement of a single point support has on the fundamental natural frequency, several cases were studied for Example 3 in Table 3. This PWB was considered general enough to be chosen for the investigation of a point support's effect on the fundamental natural frequency. One point support was placed at all the possible locations; that is, at each finite element node of the configuration obtained from the optimal solution to Example 3. This single point support is modeled as a clamped node in the finite element model; that is, both the displacement and the rotations in the x- and y-directions are zero. Each example is conducted on an 8 × 6 in. PWB that is modeled by 48 1 × 1 in. finite element squares. The total number of possible locations for the point support is 63 [(8 + 1) × (6 + 1)]. The standard finite element

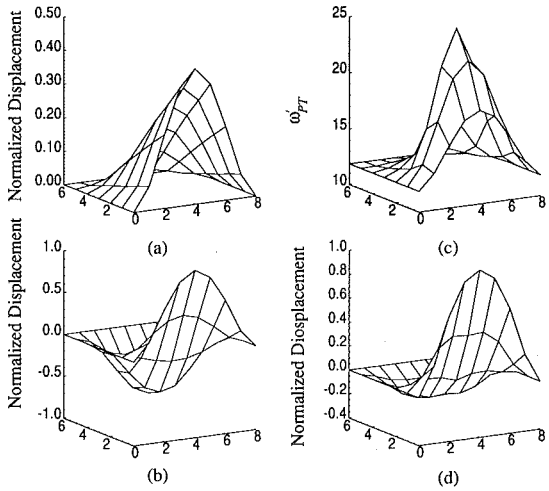

Fig. 14(*a*) Fundamental mode shape of the optimized design, (*b*) second mode shape of the optimized design, (*c*) fundamental natural frequency ω'_{PT} as a function of the location of a single clamped point support, (*d*) fundamental mode shape of the configuration with the point support placed at the location in (*c*) that corresponds to the highest value of ω'_{PT}. The boundary conditions are C-C-C-F.

method is used to obtain the mode shape corresponding to all 63 configurations, where each configuration is obtained by placing this one point support at the 63 possible locations of the plate.

To determine the location of the single point support that yields the highest increase in the fundamental natural frequency, it seems reasonable that one should place the single point support either at those locations that have the highest relative deflection amplitude of the fundamental natural frequency or at an appropriate point along the nodal line of the second mode shape [17]. In order to investigate these ideas, the eight combinations of boundary conditions given in Table 4 were studied. Consider, for example the clamped-clamped-clamped-free plate. First, the first and second mode shapes of the optimized configuration were determined. These are the shapes shown in Figs. 14(*a*) and (*b*). Then, the normalized fundamental natural frequencies $\omega'_{PT} = \omega_{PT}/\sqrt{(\rho h)_1}$ corresponding to the locations at which the point support was placed

Table 7 Effect of the single point support location on the configuration producing the maximum fundamental natural frequencies ω_1'

Boundary conditions	First two frequencies ω_1'	ω_2'	Optimal configuration with point support ω_{PT}'	Percentage improvement $100(\omega_{PT}'/\omega_1' - 1)$
C-C-C-C	22.767	35.285	39.299	79.61
S-C-S-C	20.521	27.690	30.402	48.15
C-C-C-F	11.864	21.826	24.916	110.01
C-F-C-F	9.821	12.008	14.135	43.93
C-S-F-S	8.747	15.711	16.672	90.60
C-F-S-C	6.715	18.329	19.980	197.54
S-F-S-F	3.728	7.405	9.698	160.14
S-F-F-C	3.720	9.317	10.899	192.98

were recorded. When the value of ω_{PT}' is plotted as a function of its corresponding point support location one obtains the plot shown in Fig. 14(*c*). Lastly, Fig. 14(*d*) represents the fundamental mode shape that is obtained by placing the point support at that location in Fig. 14(*c*) which yielded the highest value of ω_{PT}'. Although somewhat difficult to see in Figs. 14(*b*) and (*d*) the optimal location of the single point support yielding the highest fundamental natural frequency is coincident with one of the locations that lie along the nodal line of the second natural frequency of the optimized plate's configuration. Also, when the single point support is located at its optimal location the fundamental mode shape strongly resembles that of the second mode shape of the original optimized design for most of the boundary conditions studied. This seems to suggest that the effect of the single point support is to shift its fundamental mode shape to a mode shape that resembles that of the original second mode. The values of both the fundamental and second natural frequencies for the optimized design and the fundamental natural frequency after applying single point support at the optimal location are given in Table 7. The effect of this single support is to increase the fundamental natural frequency from 44 to 198 percent for the boundary conditions considered. The percentage improvement of ω_1' is defined as 100 $(\omega_{PT}'/\omega_1' - 1)$.

As shown in Figs. 14(*b*) and (*c*) the maximum values of ω_{PT}' occur on the nodal line of the second mode shape of the original optimal configuration. Examination of similar results for the remaining seven boundary conditions reveals that the location that has the highest relative displacement amplitude of the fundamental natural frequency is not coincident with the nodal line of the second mode shape when any of the boundaries are free. Also, the value of ω_2' and the value of ω_{PT}' are fairly close to each other, although ω_{PT}' is always greater than ω_2'. This seems to reinforce the idea that the effect of the single point support is to shift its fundamental mode shape to a mode shape that resembles that of the original optimal configuration's second mode. The optimal point support locations found for the various boundary conditions are shown in Fig. 15.

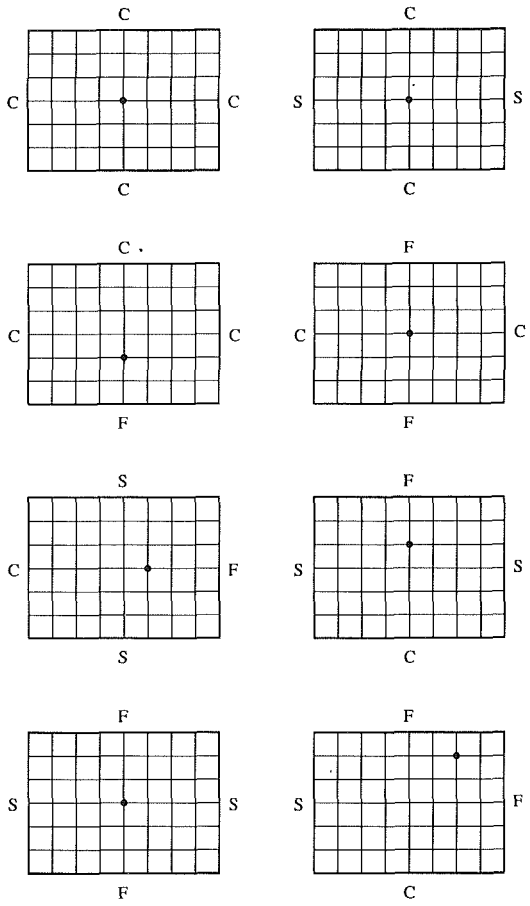

Fig. 15 Optimal point location for the configurations corresponding to the maximum natural frequencies. The symbol • denotes the point support location to obtain the maximum frequency.

Summary

A methodology to determine the configuration that gives the highest fundamental natural frequency of the PWB has been obtained by:

1. Developing a general algorithm by which the rearrangement of the CLBs is performed automatically for any combination of equal size, unequal size, movable and immovable CLBs and for all combinations of clamped, simply supported and free boundary conditions. This algorithm is also capable of incorporating two design restrictions: fixed (immovable) components and prohibited (nonswappable) areas.
2. Introducing a highly computationally efficient and accurate objective function for the evaluation of the automatic rearrangement process. Its evaluation is linearly dependent on the area of the larger of the two individual CLBs that have been selected for the interchange.
3. Adapting the simulated annealing method to solve the combinatorial rearrangement of the CLBs comprising the PWB. An empirical cooling schedule that considers the boundary conditions of the PWB and the total number of individual CLBs to be rearranged was given. Using this schedule for 61 combinations of boundary conditions, equal and unequal sized CLBs, movable and immovable CLBs, various CLB groupings and sets of materials, it was found that when compared to the exact solutions the simulated annealing method obtained the highest fundamental natural frequency within 1 percent for 87 percent of the cases considered, within 0.5 percent for 72 percent of these cases and the true maximum in 43 percent of them. The maximum discrepancy was 3 percent.

Although the method was demonstrated for boundary conditions that remained uniform along an edge, the programmed procedure can easily be generalized to include any combination of boundary conditions along a single edge, including elastically supported.

A means to determine the location of a clamped interior point support to improve upon the optimal configuration was also developed. The concept is based on the idea that the fundamental mode of the PWB with a single clamped interior point support will resemble the second mode of the optimized PWB. The optimal location of the interior point support was found by obtaining the location (node) in which the absolute value of the transverse defection for the second natural frequency was a minimum. The results confirmed that not only was the value of the fundamental natural frequency greatly

increased to values greater than those of the original second natural frequency, but the mode shapes also resembled each other. For the boundary conditions considered an additional increase in the maximum fundamental natural frequency of 44 to 198 percent was obtained.

Acknowledgment

This work was supported in part by the CALCE Electronic Packaging Research Center in the College of Engineering, University of Maryland, College Park, MD.

References

1 Rose, J., Klebsch, W., and Wolf, J., "Temperature Measurement and Equilibrium Dynamics of Simulated Annealing Placements," *IEEE Trans. Computer-Aided Design*, Vol. 9, No. 3, Mar. 1990, pp. 253–259.

2 Ying, C-S, and Wong, J. S-L, "An Analytical Approach to Floorplanning for Hierarchical Building Blocks Layout," *IEEE Trans. Computer-Aided Design*, Vol. 8, No. 4, Apr. 1990, pp. 403–412.

3 Vai, M-K, and Shanblatt, M. A., "An Improved Building Block Model for Placement using Simulated Annealing," *IEEE ISCAS*, 1987, pp. 572–575.

4 Wimer, S., and Koren, I., "Analysis of Strategies for Constructive General Block Placement," *IEEE Trans. Computer-Aided Design*, Vol. 7, No. 3, Mar. 1988, pp. 371–377.

5 Dai, W. W-M, Eschermann, B., Kuh, E. S., and Pedram, M., "Hierarchical Palcement and Floorplanning in BEAR," *IEEE Trans. Computer-Aided Design*, Vol. 8, No. 12, Dec. 1989, pp. 1335–1349.

6 Cai, H., and Hegge, J. J. A., "Comparison of Floorplanning Algorithms For Full Custom ICS," *IEEE, Custom Integrated Circuits Conference*, 1988, pp. 7.2.1–7.2.4.

7 Fukui, M., Yamamoto, A., Yamaguchi, R., Hayama, S., and Mano, Y., "A Block Interconnection Algorithm for Hierarchical Layout System," *IEEE Trans. Computer-Aided Design*, Vol. 6, No. 3, May 1987, pp. 383–394.

8 Preas, B. T., and vanCleemput, W. M., "Placement Algorithms for Arbitrarily Shaped Blocks," *IEEE 16th Design Automation Conference*, 1979, pp. 474–480.

9 Hsieh, T. M., Leong, H. W., and Liu, C. L., "Two-Dimensional Layout Compaction by Simulated Annealing," *IEEE Custom Integrated Circuits Conference*, 1988, pp. 2439–2443.

10 Breuer, M. A., "A Class of Min-Cut Placement Algorithms," *IEEE 14th Design Automation Conference*, 1977, pp. 284–290.

11 Chuowdhury, S., "Analytical Approaches to the Combinatorial Optimization in Linear Placement Problems," *IEEE Trans. Computer-Aided Design*, Vol. 8, No. 6, June 1989, pp. 630–639.

12 Valainis, J., Kaptanoglu, S., Liu, E., and Suaya, R., "Two-Dimensional IC Layout Compaction Based on Topological Design Rule Checking," *IEEE Trans. Computer-Aided Design*, Vol. 9, No. 3, March 1990, pp. 260–275.

13 Dancer, D., and Pecht, M., "Component Placement Optimization for Connectively Cooled Electronics," *IEEE Trans. on Reliability*, Vol. 38, No. 2, June 1989, pp. 199–205.

14 Knight, R. W., Goodling, J. S., and Hall, D. J., "Optimal Thermal Design of Forced Connection Heat Sinks-Analytical," ASME JOURNAL OF ELECTRONIC PACKAGING, Vol. 113, Sept. 1991, pp. 313–321.

15 Sasaki, S., and Kishimotot, T., "Optimal Structure for Microgrooved Cooling Fin for High-Power LSI Devices," *Electronics Letters*, Vol. 22, No. 25, 1986, pp. 1332–1334.

16 Osterman, M. D., and Pecht, M., "Component Placement for Reliability on Conductivity Cooled Printed Wiring Boards," ASME JOURNAL OF ELECTRONIC PACKAGING, Vol. 111, June 1989, pp. 149–156.

17 Pitarresi, J. M., and DeEdwardo, A. V., "Systematic Improvement of Support Locations for Vibrating Circuit Cards," Paper No. 91-WA/EEP-34, *ASME Winter Annual Meeting*, 1991.

18 Cheng, K-T, and Olhoff, N., "Regularized Formulation for Optimal Design of Axisymmetric Plates," *Int. J. Solids Structures*, Vol. 18, No. 2, 1982, pp. 153–169.

19 Olhoff, N., Lurie, K. A., Cherkaev, A. V., and Fedorov, A. V., "Sliding Regimes and Anisotropy in Optimal Design of Vibrating Axisymmetric Plates," *Int. J. Solids Structures*, Vol. 17, No. 10, 1981, pp. 931–948.

20 Bendsøe, M., "Some Smear-out Models for Stiffened Plates with Applications to Optimal Design," in *Int. Symposium on Optimum Structural Design*, Univ. of Arizona, Tucson, Arizona, Oct. 1981, pp. 13.29–13.34.

21 Pitarresi, J. M., Caletka, D. V., Caldwell, R., and Smith, D. E., "The Smeared Property Technique for the FE Vibration Analysis of Printed Circuit Card," ASME JOURNAL OF ELECTRONIC PACKAGING, Vol. 113, Sept. 1991, pp. 250–257.

22 Chang, T-S, and Magrab, E. B., "An Improved Procedure for the Determination of the Elastic Constants of Component-Lead-Board Assemblies," ASME JOURNAL OF ELECTRONIC PACKAGING, Vol. 113, Dec. 1991, pp. 427–430.

23 Pitarresi, J. M., and Primvera, A. A., "Comparison of Modelling Techniques for the Vibration Analysis of Printed Wiring Cards," ASME JOURNAL OF ELECTRONIC PACKAGING, Vol. 114, December 1992, pp. 378–382.

24 Burden, R. L., and Faires, D., *Numerical Analysis*, PWS Publishers, Boston, 1985.

25 Chang, T-S, "A Method to Increase the Fundamental Natural Frequency of Printed Wiring Board Assemblies," Ph.D. dissertation, University of Maryland, College Park, Maryland, 1992.

26 Kirkpatrick, S., Gelatt, Jr., C. D., and Vecchi, M. P., "Optimization by Simulated Annealing," *Science*, Vol. 220, No. 4598, 1983, pp. 671–680.

27 Metropolis, N., Rosenbluth, A. W., Rosenbluth, M. N., Teller, A. H., and Teller, E., "Equation of State of Calculations by Fast Computing Mechanics," *J. Chem. Phys.*, Vol. 21, 1953, pp. 1087–1092.